СТРУКТУРА ТА ВЛАСТИВОСТІ

STRUCTURE AND PROPERTIES

T.B. ZHELTONOZHSKAYA,
Institute of Macromolecular Chemistry NAS of Ukraine, 48, Kharkivske Shose, Kyiv, 02160, Ukraine
ORCID: 0000-0001-5272-4244
e-mail: zheltonozhskaya@ukr.net
N.M. PERMYAKOVA,
Institute of Macromolecular Chemistry NAS of Ukraine, 48, Kharkivske Shose, Kyiv, 02160, Ukraine
ORCID: 0000-0002-7622-1059
e-mail: permyakova@ukr.net
A.S. FOMENKO,
Taras Shevchenko National University of Kyiv, 60, Volodimirska str., Kyiv, 01033, Ukraine
L.R. KUNITSKAYA,
Institute of Macromolecular Chemistry NAS of Ukraine, 48, Kharkivske Shose, Kyiv, 02160, Ukraine
ORCID: 0000-0001-7027-0231
V.V. KLEPKO,
Institute of Macromolecular Chemistry NAS of Ukraine, 48, Kharkivske Shose, Kyiv, 02160, Ukraine
ORCID: 0000-0001-8089-8305
e-mail: klepko_vv@ukr.net
L.M. GRISHCHENKO,
Taras Shevchenko National University of Kyiv, 60, Volodimirska str., Kyiv, 01033, Ukraine
ORCID: 0000-0002-0342-4859
D.O. KLYMCHUK,
M.G. Kholodniy Institute of Botany NAS of Ukraine, 2, Tereshchenkivska str., Kyiv, 01601, Ukraine
ORCID: 0000-0002-7076-8213

FORMATION OF NICKEL NANOPARTICLES IN SOLUTIONS OF A HYDROPHILIC GRAFT COPOLYMER

A graft copolymer of poly(vinyl alcohol) and polyacrylamide (PVA-g-PAAm) with interacting main and grafted chains was synthesized by radical matrix polymerization of PAAm from the PVA backbone in an aqueous medium. Its basic molecular parameters including the number and length (molecular weight) of grafts were determined using elemental analysis, DTGA and viscometry. The copolymer macromolecules formed special monomolecular micelles of elipsoidal shape and length ~18-64 nm in aqueous solutions due to the formation of intramolecular polycomplexes between the main and grafted chains. This copolymer was used as a hydrophilic matrix for the in situ synthesis of nickel nanoparticles (NiNPs) in aqueous solutions. On the basis of UV-Vis spectroscopy, an original and simple method for monitoring the kinetics of the formation and yield of metal nanoparticles in systems in which a surface plasmon resonance band does not appear has been proposed and implemented. Using this approach, the kinetics of borohydride reduction of Ni-salt to NiNPs in pure water and PVA-g-PAAm solutions was studied depending on the concentrations of Ni-salt and copolymer matrices. An increase in the initial rate of accumulation and yield of NiNPs with an increase in the concentration of Ni-salt and a decrease in both parameters in copolymer solutions in comparison with pure water was established. At the same time, the accumulation rate and NiNP yield in a complex way was depended on the matrix concentration that was determined by the ratio of such factors as a decrease in the diffusion rate of $NaBH_4$ molecules in copolymer solutions and the accumulation of Ni^{2+}-ions in matrix particles due to complexation with active chemical groups at the first stage of reduction process.

T.B. Zheltonozhskaya, N.M. Permyakova, A.S. Fomenko, L.R. Kunitskaya, V.V. Klepko, L.M. Grishchenko, D.O. Klymchuk

The morphology and main structural elements of the NiNPs/PVA-g-PAAm composition were revealed using TEM. It was shown that the in situ synthesis of NiNPs in copolymer matrices was accompanied by the "detachment" of PAAm grafts from the main PVA chains and led to the appearance of two new structures, such as "hairy coils" and "hairy rods", containing small spherical NiNPs (d~0,5–12,0 nm) in isolated and chain states, respectively. The appearance of the latter structures was explained by the formation of coordination complexes of Ni^{2+}-ions with active groups of both PVA and PAAm chains at the first stage of the reduction reaction.

Key words: *graft copolymer, nickel nanoparticles, reduction process, kinetics, morphology.*

Introduction

In recent years, nickel nanoparticles (NiNPs) have become one of the most interesting and relatively cheap metallic nanomaterials due to their promising applications in chemical catalysis and electrocatalysis [1–4], in nanoelectronics as magnetic fluids [5, 6], magnetic sensors [7] and storage devices [8]. Possessing a wide range of magnetic, catalytic, biocidal, absorption, anti-inflammatory and anti-cancer properties, nickel nanoparticles are also of interest for magnetic resonance imaging [9], drug delivery, inflammatory and cancer therapy [10–13], for magnetic purification of proteins [14] and removal of toxic organic and inorganic substances from wastewater [15, 16].

Like the production of many other metal nanoparticles, there are two fundamentally different groups of methods for the synthesis of NiNPs, called "top-down" and "bottom-up" [17]. Top-down methods involve the breaking down bulk metal to nanoparticles by mechanical milling, laser ablation, nanolithography, thermal decomposition, and sputtering [18]. In the bottom-up methods, Ni-salts and Ni-oxides are used as precursors in various reactions leading to the formation of NiNPs. These are sol-gel techniques, methods of spatting, gas evaporation, co-precipitation, chemical and biochemical reduction and some other methods [19–21]. Currently, among the many ways for the formation of NiNPs, the chemical reduction of Ni-salts with sodium borohydride in solutions of polymer matrices remains one of the most popular [22]. Polymer matrices with active chemical groups first bind Ni^{2+}-ions and then prevent the aggregation of emerging NiNPs due to adsorption interaction with their surface. In addition, the polymer-assisted processes contribute to the control of the size, shape, crystallinity, oxidizability, magnetic and catalytic properties of NiNPs [23–25]. The borohydride reduction method is simple to implement; it provides fast nucleation of nanoparticles and can be carried out in various solvents at low temperatures with a good yield of metal nanoparticles.

To date, various polymers have been tested as matrices in the synthesis of NiNPs with sodium borohydride: i) synthetic homopolymers such as poly(vinyl alcohol) [22, 24], poly(vinyl pyrrolidone) [20, 23, 26, 27], poly(ethylene glycol) [28] and poly(acrylic acid) [23], ii) synthetic cross-linked polymers, for example, cation exchanged resins based on divinyl benzene with strong and weak acidic groups [29], iii) natural polymers, in particular cellulose [30] and starch [28], and iv) dendrimers and dendrimer-like hyperbranched polymers [31–34]. The main focus of these studies was on the preparation of NiNPs, identification and demonstration of their functional properties. However, such important aspects as the kinetics and detailed mechanism of these processes depending on the molecular and structural parameters of polymer matrices, the nature of the solvent and Ni-salt, temperature and relative concentrations of all components remained poorly understood.

Previously, we actively used borohydride synthesis to produce small and well stabilized silver nanoparticles (AgNPs) in aqueous solutions of some block copolymers [35–37], graft copolymers [36, 38, 39] and polymer/inorganic hybrids [36, 40, 41] containing two hydrophilic chemically complementary components, such as poly(ethylene oxide)/polyacrylamide, poly(ethylene oxide)/poly(acrylic acid), poly(vinyl alcohol)/polyacrylamide, and silica/ polyacrylamide. Due to the formation of a system of hydrogen bonds between the blocks, the backbone and grafts or between the surface of inorganic nanoparticles and grafted chains, these copolymers and hybrids formed interesting micellar and micelle-like structures that showed high stabilizing activity with respect to the emerging metal nanoparticles. It was found that the smallest AgNPs with the narrowest size distribution (2–8 nm) were formed in graft copolymer solutions [38, 39] and the resulting aqueous
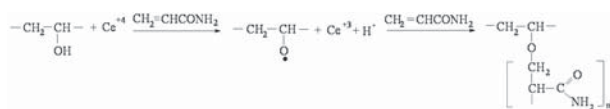
Fig. 1. Schematic representation of the graft copolymerization of PAAm from the PVA backbone

dispersions of AgNPs/PVA-*g*-PAAm remained stable in the light for over a year. Therefore, it was interesting to test this hydrophilic matrix in similar *in situ* synthesis of NiNPs.

The aim of this work was to synthesize the PVA-*g*-PAAm graft copolymer, to determine its molecular parameters, particle size and morphology in an aqueous solution, and also to study in detail the process of reduction of Ni-salt with sodium borohydride depending on the concentration of salt and copolymer matrix, as well as the structure of NiNPs/PVA-g-PAAm nanocompositions.

Experimental section

Synthesis and characterization of poly(vinyl alcohol)/polyacrylamide graft copolymer

The PVA-*g*-PAAm graft copolymer was synthesized using the well-known radical matrix polymerization of PAAm from PVA chains in aqueous medium, which was initiated by the Red/Ox reaction between Ce^{IV} ions and PVA hydroxyl groups [42]. The scheme of the polymerization reaction is shown in Figure 1. Matrix effects were caused by the interaction of growing ("daughter") PAAm chains with the main PVA chain as a matrix through the formation of a system of hydrogen bonds [43].

To synthesize the graft copolymer, we used PVA with a weight-average molecular weight M_w=90 kDa, cerium ammonium nitrate (CAN) from Aldrich (USA), and acrylamide (AAm) from Merck (Germany) re-crystallized from chloroform. The concentrations of PVA, CAN and AAm were 1.6, 0.548 and 71 kg·m^{-3}, respectively. The

reaction was carried out in deionized water and an inert atmosphere (argon) at T=20 °C and stirring during 24 hours. The gelled product was diluted with deionized water, re-precipitated with acetone, re-dissolved in water and freeze-dried.

Determining the number and length of grafted chains in graft copolymers obtained by the "grafting from" method presents a significant problem. To determine these important parameters in the case of a PVA-*g*-PAAm copolymer, we used a previously developed technique [44]. First, elemental analysis was carried out for the content of C, N and H and the weight fraction of grafts (w_{PAAm}) in the graft copolymer sample was established. Then, according to the data of dynamic thermogravimetric analysis (DTGA), the weight fraction of immobilized and adsorbed water (w_{H_2O}) was found. The next three steps were: oxidation of PVA chains in a graft copolymer of concentrated HNO$_3$, separation of low-molecular-weight products of chemical destruction of the main chains by prolonged dialysis of the reaction mixture against deionized water, and determination of the viscosity-average molecular weight (M_v) of the separated and partially hydrolyzed PAAm grafts using the well-known viscometry method. The final step was to calculate the number (N) of grafts in PVA-*g*-PAAm macromolecules using the formula (1):

$$N = \frac{w_{PAAm} \cdot M_{PVA}}{w_{PVA} \cdot M_{PAAm}}. \qquad (1)$$

The weight composition and main molecular parameters of the graft copolymer are represented in Table 1.

Morphology and size of PVA-*g*-PAAm macromolecules in aqueous solutions were established using transmission electron microscopy (TEM). For this, a JEM-I230 device (JEOL, Japan) was used, operating at an accelerating voltage of V=80 kV. Small drops (~1·10^{-4} cm^3) of the copolymer solution in

Table 1. **Main molecular parameters of the graft copolymer**

Copolymer	M_{wPVA} [1], kDa	w_{PAAm} [2], w %	w_{H_2O} [3], w %	w_{PVA} [4], w %	M_{vPAAm} [5], kDa	N [6]
PVA-*g*-PAAm	90	85,9	13,4	0,69	366	31

[1] The weight-average molecular weight of the PVA backbone. [2] The weight fraction of PAAm in the graft copolymer (according to elemental analysis for N and C). [3] The weight fraction of water (according to DTGA data). [4] The weight fraction of PVA (calculated): $w_{PVA}=1-w_{PAAm}-w_{H_2O}$. [5] The viscosity-average molecular weight of the grafts. [6] The number of grafted PAAm chains per PVA macromolecule.

deionized water were applied to copper grids coated with Formvar films and carbon. Then they were dried in air for ~1–2 min and in a vacuum desiccator for 24 hours.

Methodology of the reduction of nickel ions in copolymer solutions and pure water

The reduction of nickel ions from the $Ni(NO_3)_2 \cdot 6H_2O$ salt was carried out both in deionized water and in copolymer solutions to show the effect of the PVA-*g*-PAAm matrix on the synthesis and stabilization of NiNPs. In all cases, a significant (twenty-fold) molar excess of $NaBH_4$ with respect to Ni^{2+}-ions was used to promote their complete conversion to zero valence state. Nickel nitrate hexahydrate from Merck (Germany) and sodium borohydride from Aldrich (USA) were used. Three concentrations of the copolymer matrix (C_m=0,5; 1,0 and 2,0 kg·m^{-3}) and four concentrations of the Ni-salt ($C_{Ni(NO3)2}$=0,98·10^{-2}, 1,96·10^{-2}, 3,92·10^{-2} and 7,84·10^{-2} kg·m^{-3}) were used in these experiments.

According to a typical protocol, solutions of copolymers in deionized water were mixed with solutions of Ni-salt at T=20 °C and stored in a dark box for 1 hour; then a reducing agent was added. The reduction of solutions of Ni-salt in pure water was carried out at the same concentrations and temperatures. A few minutes after the addition of the reducing agent, the reaction mixtures turned pale gray or black depending on the concentration of the reagents, indicating the appearance of NiNPs.

Study of the formation of nickel nanoparticle by UV-Vis spectroscopy and TEM

The formation of NiNPs was monitored over time by the change in the extinction (turbidity) of each reaction mixture at λ=500 nm. At this wavelength, the Ni-salt, NiNPs and the copolymer matrix did not have absorption bands in the spectrum, and the main contribution to the extinction value was made by light scattering by the appearing metal nanoparticles. Extinction spectra were recorded every 2 minutes for 1.5 hours in the 200-1000 nm region using a Cary 50 Scan UV-Visible spectrometer from Varian (USA). Then, the values of extinction (optical density D) at λ=500 nm were used to calculate the turbidity (τ) of each reaction mixture as a function of time (t) in accordance with the well-known formula (2):

$$\tau(t) = 2{,}303\frac{D(t)}{l}, \qquad (2)$$

where l = 1 cm is the length of the quartz cell used in the experiments.

The morphology, size and shape of individual metal nanoparticles and their compositions with copolymer matrices in an aqueous medium was established by TEM. The corresponding TEM images were obtained using a JEM-I230 (JEOL, Japan) operating at an accelerating voltage of V=90 kV and the experimental technique described above. The NiNPs dispersions obtained in copolymer-free solutions were investigated as prepared using TEM. To perform similar investigations in the case of NiNPs/PVA-*g*-PAAm compositions, the reaction by-products were separated by re-precipitation of the reaction mixtures with acetone and their re-dissolution in deionized water.

Results and discussion

Morphology and size of graft copolymer nanostructures in aqueous solution

Previously, it was shown that graft copolymers PVA-*g*-PAAm form intramolecular polycomplexes (IntraPCs) within individual macromolecules in
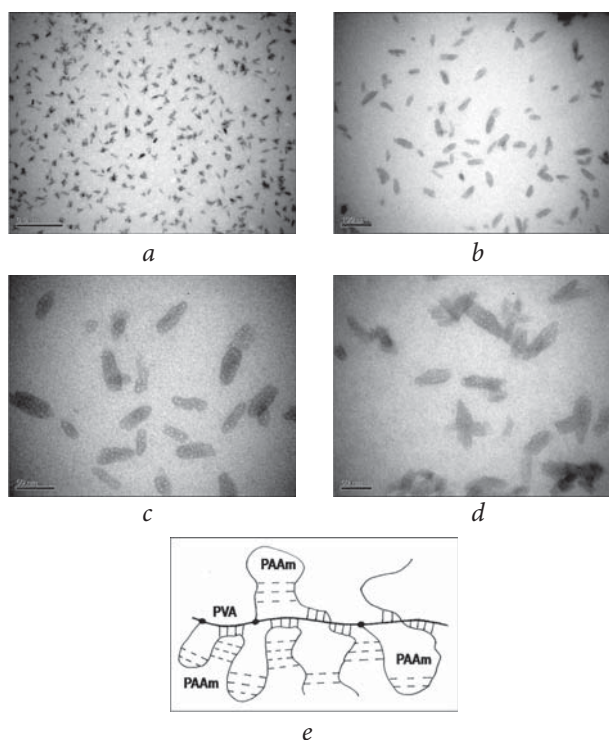

Fig. 2. Nanostructures of PVA-*g*-PAAm macromolecules in aqueous solutions shown in TEM micrographs with (*a*, *b*) lower and (*c*, *d*) higher magnification and (*e*) in the form of a schematic image. *T*=20 °C

Table 2. **Length of structural elements of the graft copolymer in aqueous solutions**

Copolymer	l, nm	
	Ellipsoidal particles	Fractal aggregates
PVA-*g*-PAAm	19–64	65–320

dilute solutions when the number and length (molecular weight) of the grafted PAAm chains does not exceed certain critical values [43]. If the number (density) of grafts in their macromolecules exceeds a certain critical value ($N > N_{cr}$), the interaction of PVA and PAAm by hydrogen bonds cannot be fully realized due to steric hindrances. However, in the case of too long grafts ($M_{PAAm} > M_{cr}$), the effect of "detaching" the grafts from the main chain is manifested [43]. The synthesized and characterized PVA-*g*-PAAm sample had such parameters N and M_{PAAm} (Table 1), which allowed the grafts to interact with the main chain [43]. Due to this, the copolymer macromolecules formed interesting ellipsoidal nanostructures in diluted aqueous solutions, which were detected using TEM (Figure 2). The PAAm chains were "pinned" to PVA backbone in these individual nanostructures by intramolecular complex formation. These nanostructures can be considered as PVA-*g*-PAAm monomolecular micelles [43].

In addition, TEM images demonstrate bizarre fractal aggregates of ellipsoidal macromolecules of the copolymer (Figure 2 **a**, **c**). The reason for their formation, apparently, lies in the surface interaction of PAAm chains (due to hydrogen bonds),

which form the "coronas" of monomolecular micelles. The sizes of individual copolymer macromolecules (monomolecular micelles) and their fractal aggregates found from TEM micrographs using the image and fax viewer are represented in Table 2. It is these PVA-*g*-PAAm nanostructures that were subsequently used as matrices for the *in situ* synthesis of NiNPs in aqueous solutions.

Monitoring the synthesis of metal nanoparticles in the absence of surface plasmon resonance effect

The formation of metal nanoparticles such as silver and gold by chemical reduction of metal ions in various media can be easily monitored using UV-Vis spectroscopy due to the appearance of intense surface plasmon resonance bands (SPRBs) with $\lambda_{max} \sim 400$ nm and ~ 520 nm, respectively [45, 46]. This method we used to characterize the kinetics of the formation of silver nanoparticles and their yield in the processes of borohydride reduction of Ag$^+$-ions in aqueous solutions of double hydrophilic block and graft copolymers and polymer/inorganic hybrids. [36, 39–41]. For this, changes in time of the position and integrated intensity of SPRB of silver nanoparticles in the UV-Vis spectra of the corresponding reaction mixtures were monitored. For some other metal nanoparticles, for example NiNPs in aqueous dispersions, SPRB is poorly expressed in the UV-Vis spectrum [47], which is explained by the less free state of surface electrons. At the same time, this band was found for NiNPs in the region of ~ 300–400 nm in some other media [21, 48, 49], but its position and
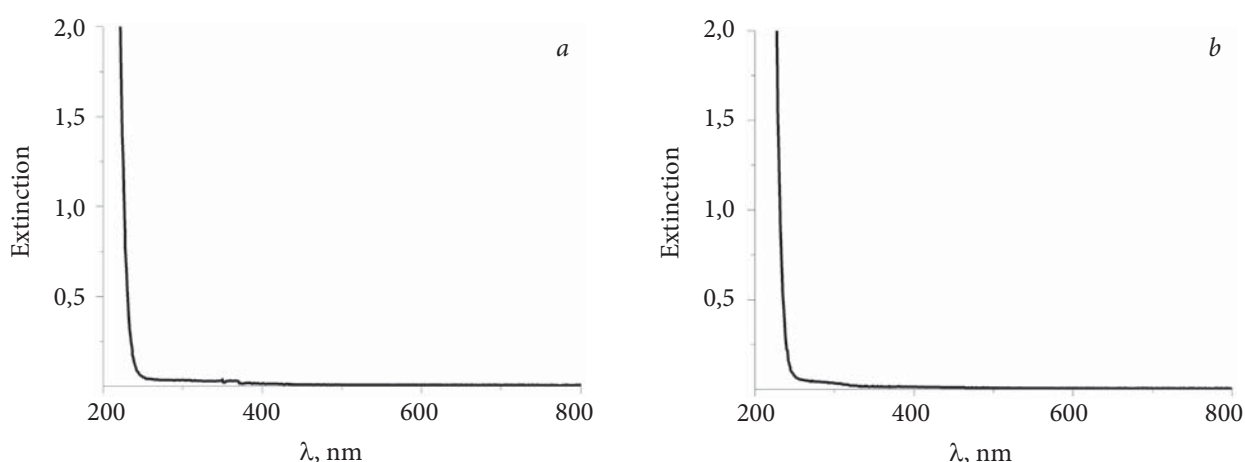

Fig. 3. Time evolution (within 90 minutes) of the extinction spectra of: (*a*) the Ni-salt aqueous solution and (*b*) its mixture with SiO$_2$-*g*-PAAm after adding NaBH$_4$. *T*=20 °C

intensity strongly depended on the size and shape of nanoparticles, as well as on the dielectric properties of the medium.

We also did not observe the appearance of SPRB in the UV-Vis spectra during the preparation of NiNPs by reduction of the Ni-salt with sodium borohydride in pure water and aqueous solutions of PVA-*g*-PAAm (in the selected range of reagent concentrations). Therefore, we looked for another way to characterize the kinetics and efficiency of the reduction process. For this, such a parameter was chosen as the turbidity of the reaction mixture at λ=500 nm. At this wavelength, aqueous solutions of Ni-salt and Ni-salt/copolymer compositions (as well as reducing agent) had no absorption bands in the spectra (Figure 3).

This meant that the extinction values at λ=500 nm in all reaction mixtures were determined only by the scattering of light on the formed metal nanoparticles. It is known that the turbidity of colloidal dispersions, which characterizes their light scattering, can be expressed for small (<λ/20 of incident light) spherical particles by the relation (3) [50]:

$$\tau = -\frac{1}{l}ln\left(\frac{I_t}{I_0}\right) = 2,303\frac{D}{l} = \left(\frac{N}{V}\right)\frac{128\cdot\pi^5\cdot a^6}{3\cdot\lambda^4}\left(\frac{n^2-1}{n^2+2}\right), \quad (3)$$

where: I_0 and I_t are the intensities of the incident and transmitted light, N/V is the number of particles per unit volume of dispersion, a is the radius of spherical particles, $n=n_1/n_2$ is the relative refractive index or the ratio of refractive indices of particles and medium. Thus, the turbidity of dispersions containing fine nanoparticles ($a<30$ nm) is determined by the size and number of scattering particles. In this case, in the considered reaction systems with formed metal nanoparticles, the change of turbidity with time (at λ=500 nm) can characterize the rate and efficiency of the reduction process. Given the formation of very small spherical NiNPs in all our reduction processes, this parameter was used to control the appearance of nanoparticles in the reaction mixtures.

Application of this approach to the synthesis of nickel nanoparticles in pure water

The reduction of Ni-salt with sodium borohydride in aqueous solutions in air can be represented by several chemical reactions [51]:
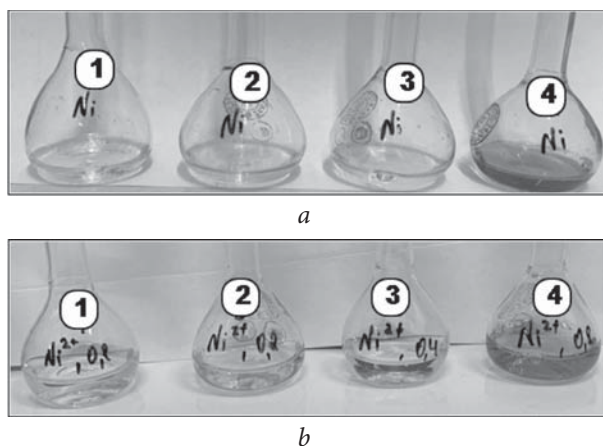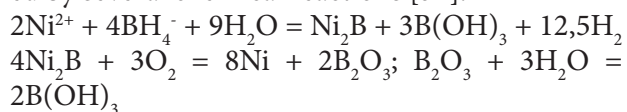
$2Ni^{2+} + 4BH_4^- + 9H_2O = Ni_2B + 3B(OH)_3 + 12,5H_2$
$4Ni_2B + 3O_2 = 8Ni + 2B_2O_3; \quad B_2O_3 + 3H_2O = 2B(OH)_3$

Fig. 4. Photographs of: (*a*) aqueous solutions of Ni-salt with increasing concentration and (*b*) mixtures of Ni²⁺/PVA-*g*-PAAm with similar concentrations of Ni-salt 10 minutes after adding NaBH₄. $C_{Ni(NO_3)_2}$=0,98·10⁻² (*1*); 1,96·10⁻² (*2*); 3,92·10⁻² (*3*) and 7,84·10⁻² kg·m⁻³ (*4*); C_m=2,0 kg·m⁻³; *T*=20 °C

Excess NaBH₄ is hydrolyzed in water according to the equation [51]:

$BH_4^- + 2H_2O = BO_2^- + 4H_2$
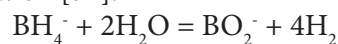
Four Ni-salt/NaBH₄ reaction mixtures with increasing $C_{Ni(NO_3)_2}$ are shown in Figure 4 (**a**).

The first three mixtures contained a less amount of NiNPs formed within 10 minutes, so they had a pale gray tint. But the latter mixture was black in color, reflecting the appearance of a large number of these nanoparticles. Extinction spectra of all mixtures recorded within 90 minutes after the start of reduction are shown in Figure 5. A bright effect of the shift of the entire spectrum along the extinction axis is seen, which was caused only by the scattering of light from the emerging NiNPs. The higher the concentration of reagents, the greater the number (or size) of the formed nanoparticles, and the greater this shift (Figure 5).

At the same time, the time dependences of turbidity obtained from these data were not monotonic in all reaction mixtures (Figure 6). Complex dependences in a number of cases can be explained by the presence of dynamic processes of aggregation/disaggregation and even partial precipitation of growing NiNPs in the measuring cell, which reflect real stochastic processes in reaction mixtures during the formation of metal nanoparticles. The kinetic curves in Figure 6 contain the induction period (the time of nucleation of nanoparticles), the length of which decreases with an increase in the concentration of Ni-salt from 28
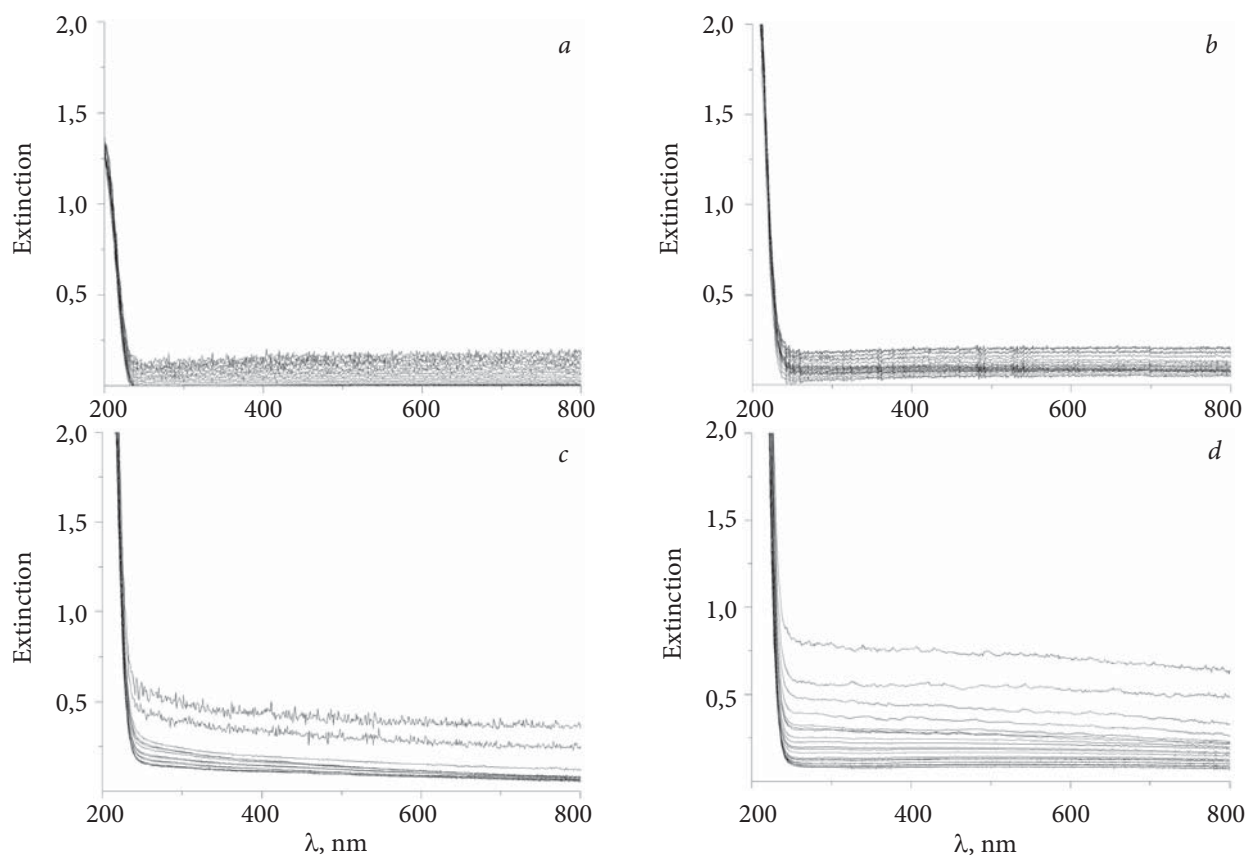
Fig. 5. Time evolution (within 90 minutes) of the extinction spectra of Ni-salt aqueous solutions after adding $NaBH_4$. Spectra are shown at interval of 4 minutes. $C_{Ni(NO_3)_2}=0{,}98\cdot10^{-2}$ (*a*); $1{,}96\cdot10^{-2}$ (*b*); $3{,}92\cdot10^{-2}$ (*c*) and $7{,}84\cdot10^{-2}$ kg·m⁻³ (*d*); $T=20$ °C

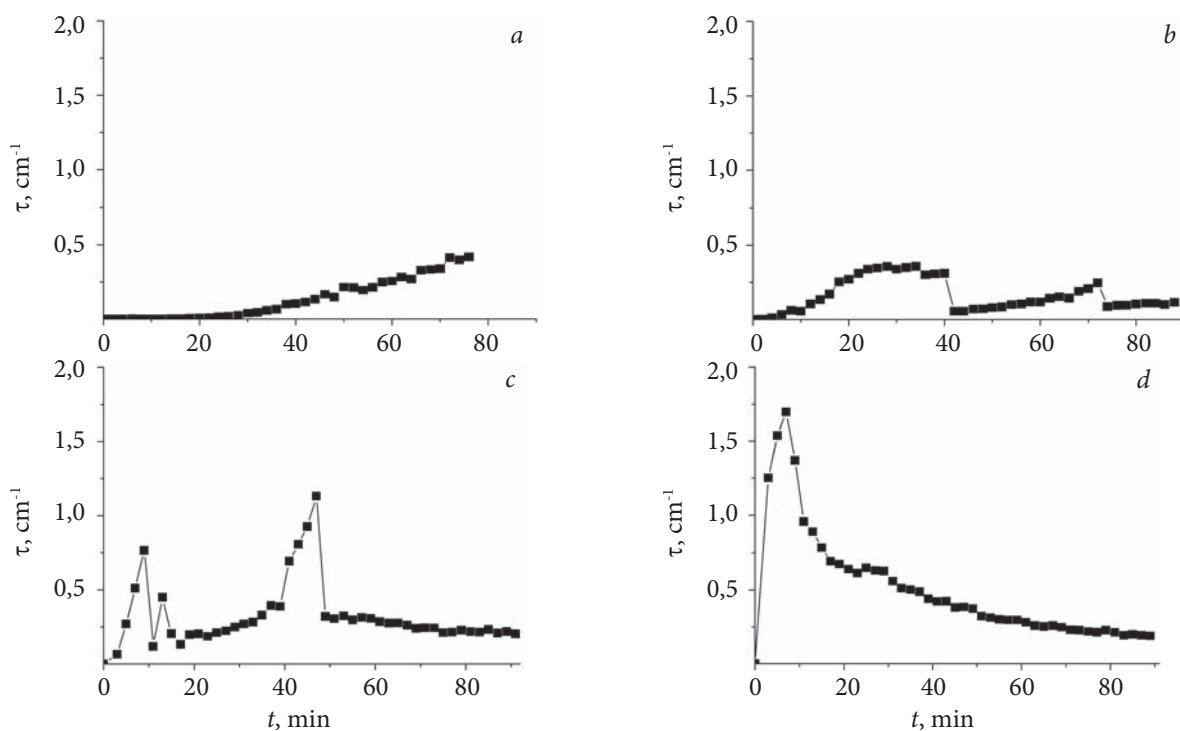**Fig. 6.** Time dependences of the turbidity of aqueous solutions of Ni-salt after adding $NaBH_4$. $C_{Ni(NO_3)_2}=0{,}98\cdot10^{-2}$ (*a*); $1{,}96\cdot10^{-2}$ (*b*); $3{,}92\cdot10^{-2}$ (*c*) and $7{,}84\cdot10^{-2}$ kg·m⁻³ (*d*); $T=20$ °C
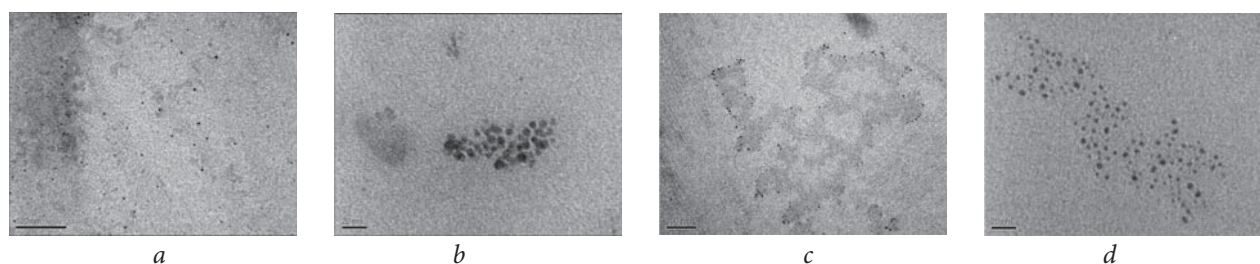
Fig. 7. TEM images of NiNPs obtained at (*a*, *b*) lowest and (*c*, *d*) highest concentrations of Ni-salt and reducing agent. $C_{Ni(NO_3)_2}$=0,98·10^{-2} (*a*, *b*) and 7,84·10^{-2} kg·m^{-3} (*c*, *d*); *T*=20 °C

minutes at $C_{Ni(NO_3)_2}$=0,98·10^{-2} kg·m^{-3} (**a**) to zero at $C_{Ni(NO_3)_2}$=7,84·10^{-2} kg·m^{-3} (**d**). In these curves, one should also note an increase in the slope of the initial portions of the time dependences of t, which indicates an increase in the initial rate of NiNP formation with an increase in the concentration of Ni-salt (and NaBH$_4$).

The formation of small spherical NiNPs even at a minimal concentration of reagents was detected by TEM (Figure 7 **a**, **b**). Their diameter varied within *d*=1–12 nm. These nanoparticles were in both isolated (Figure 7 **a**) and aggregated (Figure 7 **b**) states. Similar picture was observed at the highest concentration of reagents (Figure 7 **c**, **d**). But the size and size distribution of nanoparticles in this case were slightly lesser: *d* = 0,5–7,0 nm (Figure 7 **c**, **d**). Such result was natural given the higher rate of formation of nanoparticles at a higher concentration of reagents (Figure 6 **a**, **d**).

Analysis of the formation of nickel nanoparticles in the presence of copolymer matrices

The reduction of Ni^{2+}-ions with borohydride in PVA-*g*-PAAm solutions was carried out in two separate stages in accordance with the previously developed procedure for the *in situ* synthesis of silver nanoparticles [40,41]. At the first stage, Ni^{2+}-ions could interact with copolymer matrices due to coordination (ion-dipole) bonds with amide groups of PAAm and, probably, hydroxyl groups of the main chain of PVA. The formation of coordination complexes of Ni^{2+}-ions with PAAm chains is well known [52] (Figure 8).

At the second step, a reducing agent was added, and the reduction was monitored over time using UV-Vis spectroscopy and the same approach as for the reduction of Ni^{2+}-ions in pure water. As an example, a photograph of Ni-salt/PVA-*g*-PAAm/NaBH$_4$ reaction mixtures with constant matrix concentration and an increasing Ni-salt concentration is shown in Figure 4 (**b**). Here, the effect

of an increase in the amount of NiNPs in the reaction mixtures with an increase in $C_{Ni(NO_3)_2}$ (and reducing agent) was clearly observed. The complete series of extinction spectra recorded with 3 concentrations of copolymer matrix and 4 concentrations of Ni-salt is shown in Figure 9. In these spectra, the surface plasmon resonance bands for NiNPs also did not appear. In all reaction mixtures, only the effects of a smaller or larger shift of the extinction spectra due to light scattering by the resulting NiNPs were found. The most significant shifts along the extinction axis took place at high concentrations of Ni-salt/NaBH$_4$ and copolymer matrix (Figure 9 **j-l**), which meant the appearance of NiNPs in these mixtures with a large amount or size.

Based on the data in Figure 9, the time dependences of the turbidity of the reaction mixtures were calculated. For this, the values of extinction (optical density) at λ=500 nm were taken from the spectra and recalculated to the values of τ using formula (2). The resulting kinetic curves are shown in Figure 10. First of all, it should be noted that there are several factors that can affect the form of kinetic curves in the reaction system: Me-ions/polymer matrix/reducing agent. On the one hand, the presence of matrix particles in the reaction mixture can increase its viscosity (the higher the matrix concentration, the greater the effect)
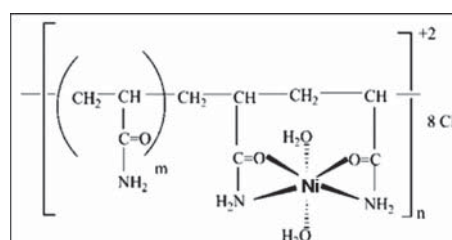

Fig. 8. Octahedral coordinative complex of Ni^{2+}-ions with PAAm chains [52]
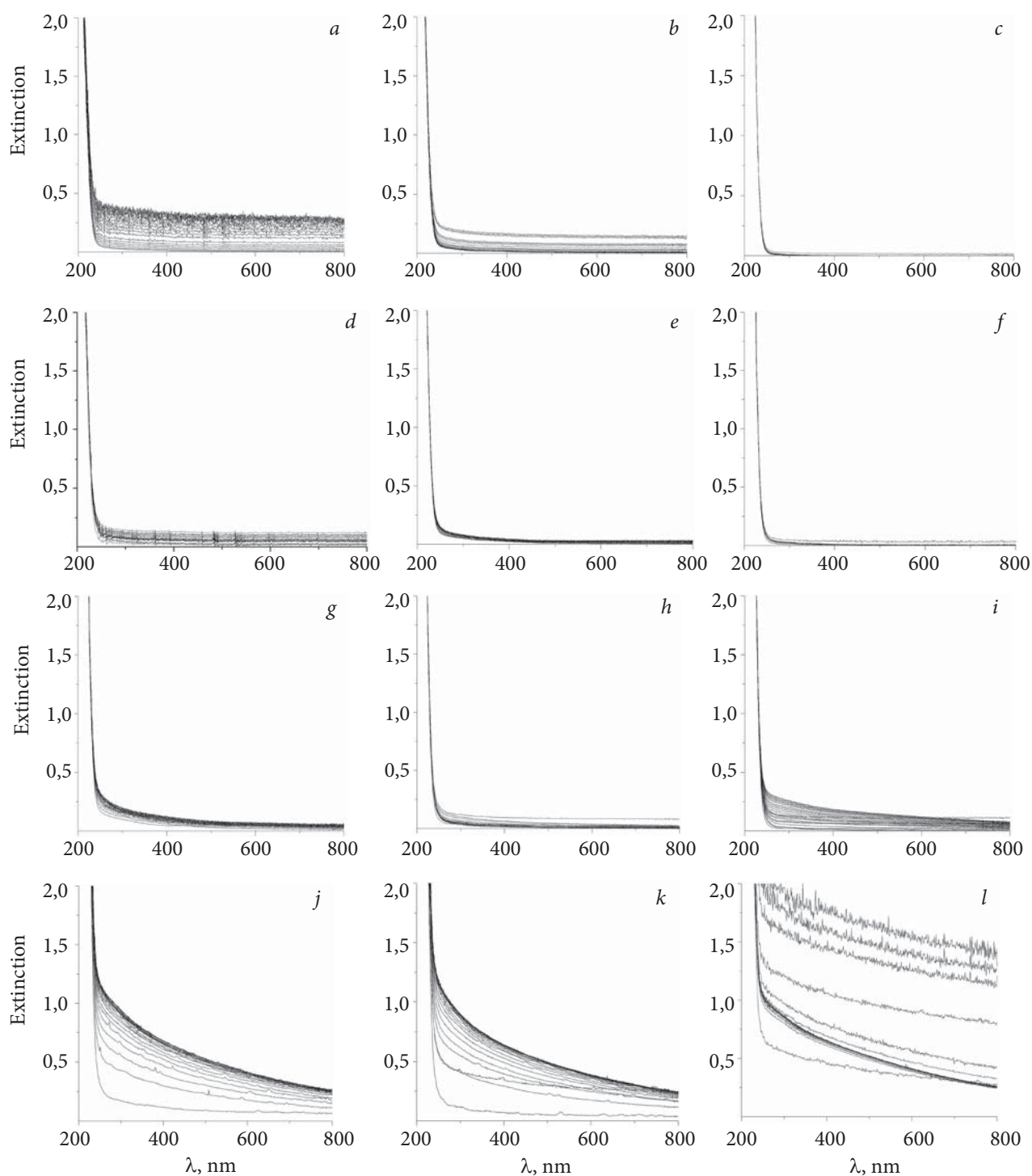
Fig. 9. Time evolution (within 90 minutes) of the extinction spectra of aqueous mixtures of Ni^{2+}/PVA-*g*-PAAm with different concentrations of Ni-salt and matrix after adding NaBH$_4$. Spectra are represented at interval of 4 minutes. $C_{Ni(NO_3)_2}$=0,98·10^{-2} (*a–c*); 1,96·10^{-2} (*d–f*); 3,92·10^{-2} (*g–i*) and 7,84·10^{-2} kg·m^{-3} (*j–l*); C_m=0,5 (*a, d, g, j*), 1,0 (*b, e, h, k*) and 2,0 kg·m^{-3} (*c, f, i, l*); *T*=20 °C

and impede the diffusion of reducing agent molecules to metal ions. On the other hand, strong local accumulation of metal ions in matrix particles due to complexation with active chemical groups at the first stage of the process can facilitate the reduction reaction. Finally, there can be real competition between the complexation of metal ions with matrices and the reaction of their reduction. Consider the kinetic curves in Figure 10 from this point of view.
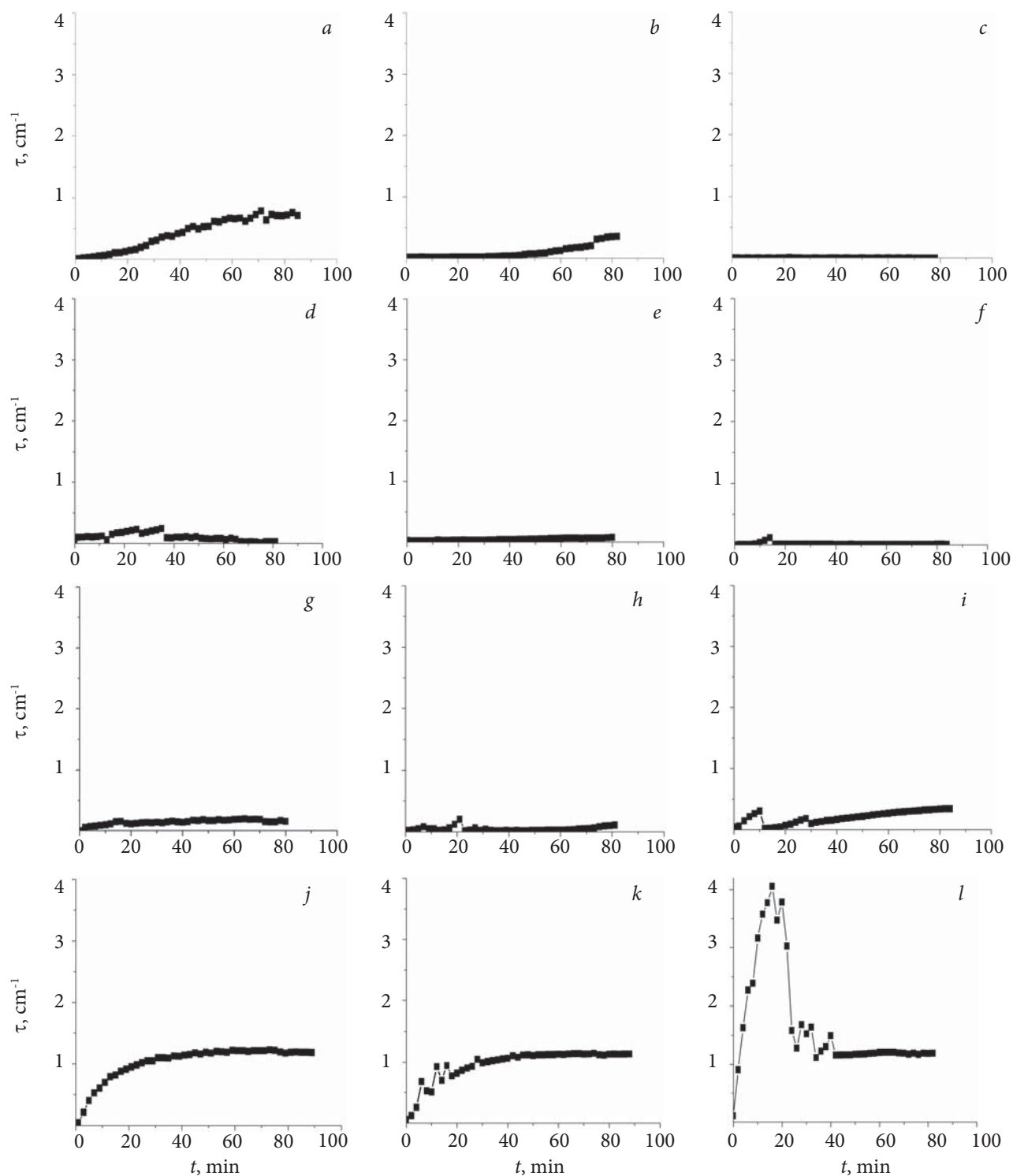
Fig. 10. Time dependences of the turbidity of Ni^{2+}/PVA-*g*-PAAm mixtures with different concentrations of Ni-salt and matrix after adding $NaBH_4$. $C_{Ni(NO_3)_2}$=0,98·10^{-2} (*a–c*); 1,96·10^{-2} (*d–f*); 3,92·10^{-2} (*g–i*) and 7,84·10^{-2} kg·m^{-3} (*j–l*); C_m=0,5 (*a, d, g, j*); 1,0 (*b, e, h, k*) and 2,0 kg·m^{-3} (*c, f, i, l*); *T*=20 °C

At low concentrations of Ni-salt ($C_{Ni(NO_3)2}$= 0,98·10^{-2} and 1,96·10^{-2} kg·m^{-3}), the reduction reaction developed more or less actively only at the lowest concentration of the copolymer matrix (Figure 10 **a**, **d**). Obviously, under such conditions, the availability of Ni^{2+}-ions bound to copolymer macromolecules at the first stage was the highest for reducing agent molecules. In this range of Ni-salt
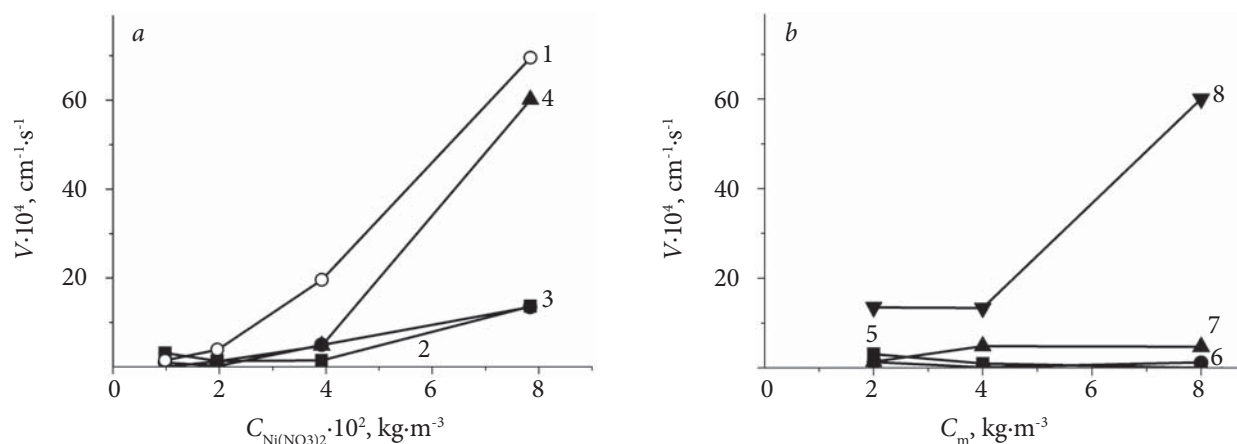
Fig. 11. The accumulation rate of NiNPs in PVA-*g*-PAAm solutions depending on: (*a*) the concentration of the Ni-salt at a constant concentration of matrix and (*b*) the concentration of the matrix at a constant concentration of the Ni-salt. $C_m=0 - 1$; $0,5 - 2$; $1,0 - 3$ and $2,0$ kg·m$^{-3} - 4$; $C_{Ni(NO_3)_2}=0,98·10^{-2} - 5$; $1,96·10^{-2} - 6$; $3,92·10^{-2} - 7$ and $7,84·10^{-2}$ kg·m$^{-3} - 8$

concentrations, an increase in copolymer concentration (and, accordingly, solution viscosity) played a negative role and reduced the rate of reduction. An active reduction reaction with a clear effect of NiNPs stabilization by PVA-*g*-PAAm macromolecules was detected in this system only at the maximum concentration of Ni-salt, $C_{Ni(NO_3)_2}=7,84·10^{-2}$ kg·m^{-3} (Figure 10 **j-l**). Here, in contrast to the region of low concentrations of Ni-salt, the initial reaction rate (determined as the slope of the initial linear portion of the corresponding kinetic curve) increased with an increase in the matrix concentration. In this case, another competitive factor from those considered above, namely: a strong accumulation of Ni^{2+}-ions by macromolecules of the copolymer and its growth with an increase in the matrix concentration, apparently played the main role in the development of the reduction reaction. But regardless of the matrix concentration, almost the same final NiNP yield was achieved (Figure 10 **j-l**). The latter conclusion was based on almost constant high values of $\tau=1,13–1,18$ cm^{-1}
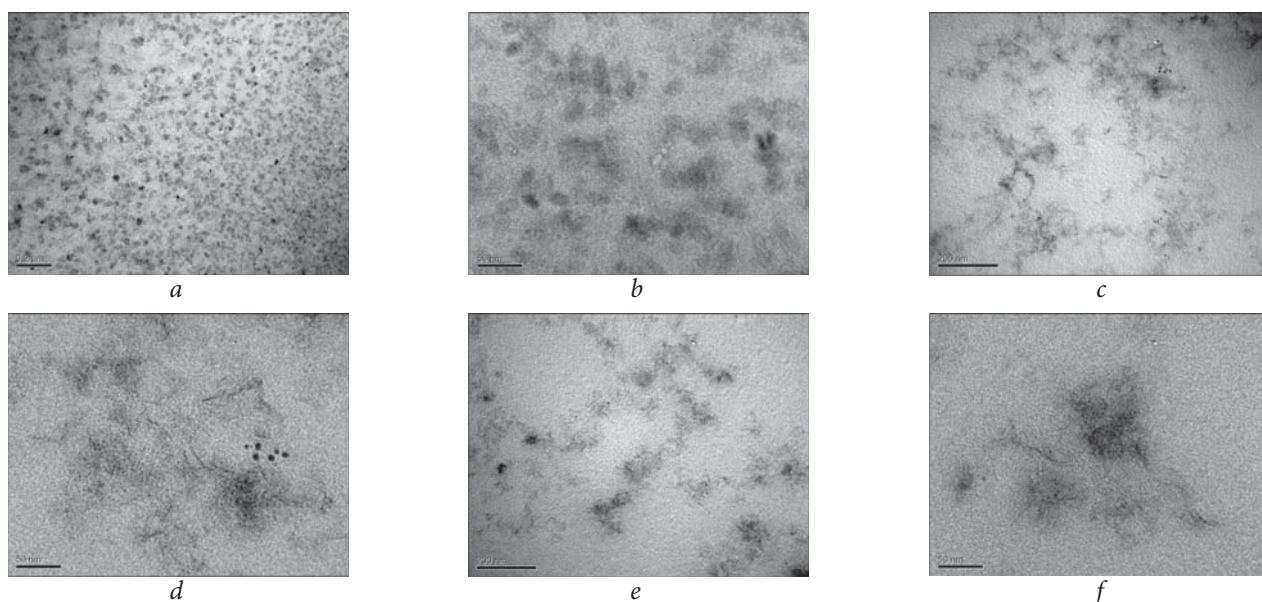

Fig. 12. TEM images of NiNPs/PVA-*g*-PAAm compositions formed in water at various concentrations of the copolymer matrix and constant concentration of the Ni-salt. $C_m=0,5$ (*a*, *b*); $1,0$ (*c*, *d*) and $2,0$ kg·m^{-3} (*e*, *f*); $C_{Ni(NO_3)_2}=7,84·10^{-2}$ kg·m^{-3}; $T=20$ °C

Table 3. **Sizes of separate structural elements of the compositions**

Composition	C_m, kg·m^{-3}	$C_{Ni(NO_3)_2}\cdot10^2$, kg·m^{-3}	$d^{1)}$, nm		$l^{2)}$, nm
			"hairy coils"	NiNPs	"hairy rods"
NiNPs/PVA-*g*-PAAm	0,5		11–70	0,5–3,0	–
	1,0	7,84	12–77	1–8	14–66
	2,0		11–59	1–12	10–36

$^{1)}$ Diameters of "hairy coils" and nickel nanoparticles included in them. $^{2)}$ Length of "hairy rods" containing NiNP chains.

on all kinetic curves after a certain constant time (80 minutes). Here, the highly stabilizing role of the copolymer matrix with respect to NiNPs was fully manifested. It should be noted that the term "yield" of NiNPs should only be understood as the accumulation of the total mass of nanoparticles, since in these cases it was impossible to separate the contributions to turbidity from the number of particles and their size.

Figure 11 compares the initial rates of NiNPs accumulation in different reaction mixtures in the absence and in the presence of stabilizing copolymer matrices. As can be seen, an increase in the concentration of Ni-salt (and NaBH$_4$) in the reaction mixture led to an increase in the rate of formation of NiNPs (Figure 11 **a**). This picture was retained both in pure water (curve *1*) and in copolymer solutions at all studied concentrations (curves *2–4*). Attention should also be paid to the more intensive development of the reduction process in pure water in comparison to copolymer solutions (curve *1* in comparison with curves *2–4*). This fact can be explained by the action of the above factors, such as a decrease in the diffusion rate of NaBH$_4$ molecules in copolymer solutions and strong complexation of Ni^{2+}-ions with PAAm (and PVA) chains in PVA-*g*-PAAm macromolecules (monomicelles), which competes with reduction. An increase in the matrix concentration (at a constant concentration of Ni-salt and a reducing agent) had different effects on the accumulation rate of nanoparticles (Figure 11 **b**) depending on the salt concentration. This can be seen as a result of the predominant action of one or the other of the previously noted factors, as discussed above.

The morphology of NiNPs/PVA-*g*-PAAm compositions with different concentrations of copolymer matrices and the highest concentration of Ni-salt is shown in the TEM images in Figure 12. For these studies, each reaction mixture was pu-

rified from the reduction by-products 90 minutes after the start of the reaction by reprecipitation with ethanol and redissolution in deionized water. These images showed, firstly, the presence of very small dark NiNPs in the PVA-*g*-PAAm macrocoils, and, secondly, changes in the state of the macromolecules themselves caused by the formation of NiNPs. Indeed, individual copolymer macromolecules no longer resembled well-defined elongated (ellipsoidal) structures, as it was before the synthesis of NiNPs in them (Figure 2). In the final compositions, two morphological forms of copolymer macromolecules were observed. They can be called "hairy coils" and "hairy rods". In the first structure, many small NiNPs were located mainly in the center of the coil, which had a shape close to spherical (Figure 12 **a**, **b**), while the central place of the other structure was occupied by NiNPs chains (rods) (dark lines in Figure 12 **c-e**). The appearance of such "hairy" structures indicated the detachment of PAAm grafts from the main PVA chains during the *in situ* synthesis of NiNPs. The relative content and sizes of these structures in the compositions depended on the ratio of the concentrations of the Ni-salt and copolymer matrices. When this ratio was high ($C_{Ni(NO_3)_2}/C_m$=0,16 w/w), the composition mainly contained "hairy coils" (Figure 12 **a**, **b**). But if the relative content of Ni-salt in the compositions decreased ($C_{Ni(NO_3)_2}/C_m$=0,08 and 0,04 w/w), "hairy rods" also appeared (Figure 12 **c-e**). The appearance of the latter structures in the compositions made it possible to conclude that, at the first stage of the reduction reaction, a certain fraction of Ni^{2+}-ions penetrated deeper into the matrix particles and formed coordinative complexes with both the main and grafted chains. As a result, when the reducing agent was added, small NiNPs could form right along the main chain, creating a kind of rods. In addition, all TEM images also contained various aggregates of point structures.

The sizes of individual structures, estimated from the images in Figure 12, are presented in Table 3.

Concluding remarks

The graft copolymer PVA-*g*-PAAm was synthesized using the radical matrix polymerization of PAAm from the PVA backbone in an aqueous medium. Its chemical composition and basic molecular parameters including the number and molecular weight (length) of grafted chains (N=31 and M_{vPAAm}=366 kDa) were determined using elemental analysis, DTGA and viscometry. Individual macromolecules of the copolymer, which can be attributed to monomolecular micelles, had an elongated (elipsoidal) shape in aqueous solutions with a length of ~18–64 nm due to the formation of intramolecular polycomplexes between the main and grafted chains. These macromolecules (or monomicelles) also formed bizarre fractal aggregates of various sizes and shapes.

An original method for monitoring the kinetics of the formation of metal nanoparticles in systems in which a surface plasmon resonance band does not appear in UV-Vis spectra has been proposed, physically substantiated, and implemented. Based on this approach, the kinetics of borohydride reduction of Ni^{2+}-ions in deionized water and aqueous solutions of PVA-*g*-PAAm was studied and analyzed depending on the concentrations of Ni-salt and copolymer matrices. The effects of an increase in the initial accumulation rate and yield of NiNPs with an increase in the concentration of Ni-salt and a deceleration of the reduction of metal ions in copolymer solutions in comparison with pure water (due to the complexation of Ni^{2+}-ions with amide and hydroxyl groups of PAAm and PVA) were established. At the same time, the accumulation rate and NiNPs yield in a complex way was depended on the matrix concentration that was determined by the ratio of such factors as a decrease in the diffusion rate of $NaBH_4$ molecules in copolymer solutions and the accumulation of Ni^{2+}-ions in matrix particles due to complexation with active chemical groups at the first stage of reduction process.

The morphology and main structural elements of the NiNPs/PVA-*g*-PAAm composition were revealed. It was shown that the *in situ* synthesis of NiNPs in copolymer matrices was accompanied by the "detachment" of PAAm grafts from the main PVA chains and led to the appearance of two new structures, such as "hairy coils" and "hairy rods", containing small spherical NiNPs (*d*~0,5–12,0 nm) in isolated and chain states, respectively. The design and size of these structures depended on the relative content of the Ni-salt in the composition. Structures of the "hairy coil"-type with a diameter of ~10–77 nm and small NiNPs, located mainly in the centers of the coils, prevailed in the composition at a high relative content of Ni-salt (0,16 w/w), while the structures of "hairy rods" having a length of ~10–66 nm and containing NiNP chains, appeared at a lower relative content of Ni-salt (0,08 and 0,04 w/w). The appearance of the latter structures was attributed to the formation of coordination complexes of Ni^{2+}-ions with active groups of both PVA and PAAm chains at the first stage of the reduction reaction.

REFERENCES

1. *Alonso F., Riente P., Yus M.* Hydrogen-transfer reduction of carbonyl compounds promoted by nickel nanoparticles. Tetrahedron, 2008, **64**: 1847–1852. https://doi.org/10.1016/j.tet.2007.11.093.

2. *Abbas S.A., Ma A., Seo D., Lim Y.J., Jung K.-D., Nam K.M.* Application of spiky nickel nanoparticles to hydrogen evolution reaction. Bull. Korean Chem. Soc., 2020 (6 pp.). DOI: 10.1002/bkcs.12113.

3. *Metin Ö., Mazumder V., Özkar S., Sun S.* Monodisperse nickel nanoparticles and their catalysis in hydrolytic dehydrogenation of ammonia borane. J. Am. Chem. Soc., 2010, **132**: 1468–1469. https://doi.org/10.1021/ja909243z.

4. *Zhiani M., Kamali S.* Preparation and evaluation of nickel nanoparticles supported on the polyvinylpyrrolidone-graphene composite as a durable electrocatalist for HER in alkaline media. Electrocatalysis, 2016, **7**: 466–476. https://doi.org/10.1007/s12678-016-0330-1.

5. *Vekas L., Avdeev M.V., Bica D.* Magnetic nanofluids: synthesis and structure. In: Nanoscience in Biomedicine, Shi, D. (Ed.), Chapter 25, Springer-Verlag: Berlin, 2009, 650. https://doi.org/10.1007/978-3-540-49661-8_25.

6. *Moumen A., Fattouhi M., Abderrafi K., El Hafidi M., Ouascit S.* Nickel colloid nanoparticles: synthesis, characterization, and magnetic properties. J. Cluster Sci., 2019, **30**: 581–588. https://doi.org/10.1007/s10876-019-01517-8.

7. *Wang Z.K., Kuok M.H., Ng S.C., Lockwood D.J., Cottam M.G., Nielsch K., Wehrpohn R.B., Gosele U.* Spin-wave

quantization in ferromagnetic nickel nanowires. Phys. Rev. B, 2002, **89**: Art. 27201. https://doi.org/10.1103/PhysRev-Lett.89.027201.

8. *Murray C.B., Sun S., Doyle H., Betley T.* Monodisperse 3d transition metal (Co, Ni, Fe) nanoparticles and their assembly into nanoparticle superlattice. Mrs. Bulletin, 2001, **26**: 985–991. https://doi.org/10.1557/mrs2001.254.

9. *Mornet S., Vasseur S., Grasset F., Veverka P., Goglio G., Demourgues A., Portier J., Pollert E., Duguet E.* Magnetic nanoparticle design for medical applications. Prog. Solid State Chem., 2006, **34**: 237–247. https://doi.org/10.1016/j.progsolidstchem.2005.11.010.

10. *Guo D., Wu C., Hu H., Wang X., Li X., Chen B.* Study on the enhanced cellular uptake effect of daunorubicin on leukemia cells mediated via functionalized nickel nanoparticles. Biomed. Mater., 2009, **4**: Art. 025013. https://doi.org/10.1088/1748-6041/4/2/025013.

11. *Tietze R., Zaloga J., Unterwegen H., Lyer S., Friedrich R.P., Janko C., Pottler M., Durr S., Alexiou C.* Magnetic nanoparticle-based drug delivery for cancer therapy. Biochem. Biophys. Res. Commun., 2015, **468**: 463–470. https://doi.org/10.1016/j.bbrc.2015.08.022.

12. *Chen M., Zhang Y., Huang B., Yang X., Wu Y., Liu B., Yuan Y., Zhang G.* Evaluation of the antitumor activity by Ni nanoparticles with verbascoside. J. Nanomater., 2013, **2013**: Art. 623497. https://doi.org/10.1155/2013/623497.

13. *Angajala G., Radhakrishnan S.* A review on nickel nanoparticles as effective therapeutic agents for inflammation. Inflammation & Cell Signaling, 2014, **1**: Art. e271. https://doi.org/10.14800/ics.271.

14. *Parisien A., Al-Zarka F., Hussack G., Baranova E.A., Thibault J., Lan, C.Q.* Nickel nanoparticles synthesized by a modified polyol method for the purification of histidine-tagged single-domain antibody ToxA5.1. J. Mater. Res., 2012, **27**: 2884–2890. https://doi.org/10.1557/jmr.2012.323.

15. *Pandian C.J., Palanivel R., Dhananasekaran S.* Green synthesis of nickel nanoparticles using *Ocimum sanctum* and their application in dye and pollutant adsorption. Chinese J. Chem. Eng., 2015, **23**: 1307–1315. https://doi.org/10.1016/j.cjche.2015.05.012.

16. *Zhang G., Li J., Zhang G., Zhao L.* Room-temperature synthesis of Ni nanoparticles as the absorbent used for sewage treatment. Adv. Mater. Sci. Eng., 2015, **2015**: Art. 973648. https://doi.org/10.1155/2015/973648.

17. *Jaji N.-D., Lee H.L., Hussin M.H., Akil H.M., Zakaria M.R., Othman M.B.H.* Advanced nickel nanoparticle technology: from synthesis to application. Nanotechnol. Rev., 2020, **9**: 1456–1480. https://doi.org/10.1515/ntrev-2020-0109.

18. *Ealias A.M., Saravanakumar M.* A review on the classification, characterization, synthesis of nanoparticles and their application. IOP Conf. Ser. Mater. Sci. Eng., 2017, **263**: 32019–32032. https://doi.org/10.1088/1757-899X/263/3/032019.

19. *Chen D.H., Wu S.H.* Synthesis of nickel nanoparticles in water-in-oil microemulsions. Chem. Mater., 2000, **12**: 1354–1360. https://doi.org/10.1021/cm991167y.

20. *Pandey A., Manivannan R.* Chemical reduction technique for the synthesis of nickel nanoparticles. Int. J. Eng. Res. Appl., 2015, **5**: 96–100. https://doi.org/10.2174/1877912305666150417232717.

21. *Din M.I., Rani A.* Recent advances in the synthesis and stabilization of nickel and nickel oxide nanoparticles: a green adeptness. Int. J. Anal. Chem., 2016, **2016**: Art. 3512145. https://doi.org/10.1155/2016/3512145.

22. *Li J., Lee K.-P., Gopalan A.I.* One-step preparation of nickel nanoparticle-based magnetic poly(vinyl alcohol) gels. Coatings, 2019, **9**: Art. 744. DOI: 10.3390/coatings9110744. https://doi.org/10.3390/coatings9110744.

23. *Roy P.S., Bhattacharya S.K.* Size-controlled synthesis, characterization and electrocatalytic behaviors of polymer-protected nickel nanoparticles: a comparison with respect to two polymers. RSC Adv., 2014, **4**: 13892–13900. https://doi.org/10.1039/C4RA00426D.

24. *Singh V., Srinivas V., Ranot M., Angappane S., Park J.-G.* Effect of polymer coating on the magnetic properties of oxygen-stabilized nickel nanoparticles. Phys. Rev. B, 2010, **82**: Art. 054417. https://doi.org/10.1103/PhysRevB.82.054417.

25. *Farooqi Z.H., Iqbal S., Khan S.R., Kanwal F., Begum R.* Cobalt and nickel nanoparticles fabricated p(NIPAM-co-MAA) microgels for catalytic applications. e-Polymers, 2014, **14**: 313–321. https://doi.org/10.1515/epoly-2014-0111.

26. *Couto G.G., Klein J.J., Schreiner W.H., Mosca D.H., de Oliveira A.J.A., Zarbin A.J.G.* Nickel nanoparticles obtained by a modified polyol process: synthesis, characterization, and magnetic properties. J. Coll. Interface Sci., 2007, **311**: 461–468. https://doi.org/10.1016/j.jcis.2007.03.045.

27. *Demidova Y., Simakova I., Prosvirin I., Murzin D.Yu., Simakov A.* Size-controlled synthesis of Ni and Co metal nanoparticles by the modified polyol method. Int. J. Nanotechnol., 2016, **13**: 1/2/3: 3–14. https://doi.org/10.1504/IJNT.2016.074519.

28. *Anurai S., Tejanhiram Y., Mahdiyar B., Shivaraman R., Gopalakrishnan C., Karthigeyan A.* Wet chemical synthesis of nickel nanostructures using different capping agents. Asian J. Chem. 2013, **25**: Suppl. Iss.: 65–68.

29. *Gopalan E.V., Malini K.A., Santhoshkumar G., Narayanan T.N., Joy P.A., Al-Omari I.A., Kumar D.S., Yoshida Y., Anantharaman M.R.* Template-assisted synthesis and characterization of passivated nickel nanoparticles. Nanoscale Res. Lett. 2010, **5**: 889–897. https://doi.org/10.1007/s11671-010-9580-7.

30. *Pirkkalainen K., Vainio U., Kisko K., Elbra T., Kohout T., Kotelnikova N.E., Serimaa R.* Structure of nickel nanoparticles in a microcrystalline cellulose matrix studied using anomalous small-angle X-ray scattering. J. Appl. Cryst., 2007, **40**: 489–494. https://doi.org/10.1107/S0021889806055804.

31. *Mazumder A., Davis J., Rangari V., Curry M.* Synthesis, characterization, and applications of dendrimer-encapsulated zero-valent Ni nanoparticles as antimicrobial agents. Int. Scholarly Res. Notices, 2013, **2013**: Art. 843709. https://doi.org/10.1155/2013/843709.

32. *Knecht M.R., Garcia-Martinez J.C., Crooks R.M.* Synthesis, characterization, and magnetic properties of dendrimer-encapsulated nickel nanoparticles containing <150 atoms. Chem. Mater. 2006, **18**: 5039–5044. https://doi.org/10.1021/cm061272p.

33. *Kalbasi R.J., Zamani F.* Synthesis and characterization of Ni nanoparticles incorporated into hyperbranched poly-amidoamine-polyvinylamine/SBA-15 catalist for simple reduction of nitro aromatic compounds. RSC Adv., 2014, **4**: 7444–7453. https://doi.org/10.1039/c3ra44662j.

34. *Zhu Z., Guo X., Wu S., Zhang R., Wang J., Li L.* Preparation of nickel nanoparticles in spherical polyelectrolyte brush nanoreactor and their catalytic activity. Ind. Eng. Chem. Res. 2011, **50**: 13848–13853. https://doi.org/10.1021/ie2017306.

35. *Permyakova N.M., Zheltonozhskaya T.B., Poguliai Y.V.* Micelle formation and stabilization of metal nano-particles in aqueous solutions of diblock copolymers with poly(acrylic acid) and poly(ethylene oxide). Mol. Cryst. Liq. Cryst., 2011, **536**: 372–379. https://doi.org/10.1080/15421406.2011.538589.

36. *Fedorchuk S., Zheltonozhskaya T., Gomza Yu., Kunitskaya L., Demchenko O.* Synthesis of silver nano-particles in the matrices of block and graft copolymers and polymer-inorganic substances in water. Macromol. Symp., 2012, **317–318**: 103–116. https://doi.org/10.1002/masy.201100098.

37. *Fedorchuk S.V., Zheltonozhskaya T.B., Gomza Yu.P., Klymchuk D.O., Kunitskaya L.R.* Morphology of silver nanoparticles in the micelle-forming block copolymers. Mol. Cryst. Liq. Cryst., 2014, **590**: 172–178. https://doi.org/10.1080/15421406.2013.874213.

38. *Fedorchuk S.V., Zheltonozhskaya T.B., Gomza Yu.P., Nessin S.D., Klymchuk D.O.* Morphology of silver nanoparticles in the graft copolymer matrices. J. Proc. Int. Conf. "Nanomaterials: Applications and Properties", 2013, **2**: Art. 02PCN31.

39. *Zheltonozhskaya T.B., Fedorchuk S.V., Klymchuk D.O., Gomza Yu.P., Nessin S.D.* Graft copolymers PVA-*g*-PAAm as effective matrices for the formation and stabilization of silver nanoparticles. Polymeric J., 2016, **38**: 244–254 (in Ukrainian).

40. *Zheltonozhskaya T.B., Permyakova N.M., Kondratiuk T.O., Beregova T.V., Klepko V.V., Melnik B.S.* Hybrid-stabilized silver nanoparticles and their biological impact on hospital infections, healing wounds, and wheat cultivation. French-Ukainian J. Chem., 2019, **7**: 20–39. https://doi.org/10.17721/fujcV7I2P20-39.

41. *Zheltonozhskaya T.B., Permyakova N.M., Kravchenko O.O., Maksin V.I., Nessin S.D., Klepko V.V., Klymchuk D.O.* Polymer/inorganic hybrids containing silver nanoparticles and their activity in the disinfection of fish aquariums/ponds. Polym.-Plast. Technol. Mater., 2021, **60**: 369–391. https://doi.org/10.1080/25740881.2020.1811318.

42. *Zheltonozhskaya T.B., Zagdanskaya N.E., Demchenko O.V., Momot L.N., Permyakova N.M., Syromyatnikov V.G., Kunitskaya L.R.* Graft copolymers with chemically complementary components as a special class of high-molecular-weight compounds. Russ. Chem. Rev., 2004, **73**: 811–829. https://doi.org/10.1070/RC2004v073n08ABEH000901.

43. *Zheltonozhskaya T., Permyakova N., Momot L.* Intramolecular polycomplexes in block and graft copolymers. Ch.5. In: Hydrogen-Bonded Interpolymer Complexes. Formation, Structure and Application. Eds. Khutoryanskiy V. and Staikos G. New Jersey–London–Singapore etc.: World Scientific, 2009: 85–153. https://doi.org/10.1142/9789812709776_0005.

44. *Zheltonozhskaya T.B., Permyakova N.M., Kunitskaya L.R., Klymchuk D.O.* Synthesis of the micellar nanocontainers and nanoreactors based on the block and graft copolymers and polymer/inorganic hybrids. Ch. 1.3. In: Multifunctional nanomaterials for biology and medicine: molecular design, synthesis, and application. Ed. R.S. Stoika, Kyiv: Nauk. Dumka, 2017: 36–67 (in Ukrainian).

45. *Kelly K.L., Coronado E., Zhao L.L., Schatz G.C.* The optical properties of metal nanoparticles: the influence of size, shape, and dielectric environment. J. Phys. Chem. B., 2003, **107**: 668–677. https://doi.org/10.1021/jp026731y.

46. *Liz-Marzan L.M.* Tailoring surface plasmons through the morphology and assembly of metal nanoparticles. Langmuir, 2006, **22**: 32–41. https://doi.org/10.1021/la0513353.

47. *Yershov B.G.* Metal nanoparticles in aqueous solutions: electronic, optical and catalytic properties. Rus. Chem. J., 2001, **XLV**: 20–30 (in Russian).

48. *Sharma V., Chotia C., Tarachand, Ganesan T.V., Okram G.S.* Influence of particle size and dielectric environment on the dispersion behaviour and surface plasmon in nickel nanoparticles. Phys. Chem. Chem. Phys., 2017, **19**: 14096–14106. https://doi.org/10.1039/C7CP01769C.

49. *Mamuru S.A., Jaji N.* Voltammetric and impedimetric behaviour of phytosynthesized nickel nanoparticles. J. Nano-

struct. Chem., 2015, **5**: 347–356. https://doi.org/10.1007/s40097-015-0166-x.

50. *Wainwright E.* Particle size characterization in turbid colloidal suspensions. Physics Department, The College of Wooster, Ohio, USA, 2014, 7. http://physics.wooster.edu/JrIS/Files/Web_Article_Wainright.pdf.

51. *Glavee G.N., Klabunde K.J., Sorensen C.M., Hadjipanayis G.C.* Borohydride reduction of nickel and copper ions in aqueous and nonaqueous media. Controllable chemistry leading to nanoscale metal and metal boride particles. Langmuir, 1994, **10**: 4726–4730. https://doi.org/10.1021/la00024a055.

52. *Sari N., Kahraman E., Sari B., Özgün A.* Synthesis of some polymer-metal complexes and elucidation of their structures. J. Macromol. Sci., Part A: Pure Appl. Chem., 2006, **43**: 1227–1235. https://doi.org/10.1080/10601320600737484

Т.Б. Желтоножська,
Інститут хімії високомолекулярних сполук НАН України, Харківське шосе 48, 02160 Київ, Україна
e-mail: zheltonozhskaya@ukr.net

Н.М. Пермякова,
Інститут хімії високомолекулярних сполук НАН України, Харківське шосе 48, 02160 Київ, Україна
e-mail: permyakova@ukr.net

А.С. Фоменко,
Київський національний університет імені Тараса Шевченка, вул. Володимирська 60, 01033 Київ, Україна

Л.Р. Куницька,
Інститут хімії високомолекулярних сполук НАН України, Харківське шосе 48, 02160 Київ, Україна

В.В. Клепко,
Інститут хімії високомолекулярних сполук НАН України, Харківське шосе 48, 02160 Київ, Україна
e-mail: klepko_vv@ukr.net

Л.М. Гріщенко,
Київський національний університет імені Тараса Шевченка, вул. Володимирська 60, 01033 Київ, Україна

Д.О. Клімчук,
Інститут ботаніки ім. М.Г. Холодного НАН України, вул. Терещенківська 2, 01601 Київ, Україна

УТВОРЕННЯ НАНОЧАСТИНОК НІКЕЛЮ В РОЗЧИНАХ ГІДРОФІЛЬНОГО ПРИЩЕПЛЕНОГО КОПОЛІМЕРУ

Прищеплений кополімер полівінілового спирту та поліакриламіду (ПВС-*g*-ПАА) із взаємодіючими основним і прищепленими ланцюгами синтезовано методом радикальної матричної полімеризації ПАА від основного ланцюга ПВС у водному середовищі. Методами елементного аналізу, ДТГА та віскозиметрії визначено його основні молекулярні параметри, включаючи кількість та довжину (молекулярну масу) щеплень. Макромолекули кополімеру у водних розчинах утворювали особливі мономолекулярні міцели еліпсоїдальної форми довжиною ~18–64 нм за рахунок утворення інтрамолекулярних полікомплексів між основним і прищепленими ланцюгами. Цей кополімер було використано як гідрофільну матрицю для *in situ* синтезу наночастинок нікелю (NiНЧ) у водних розчинах. На основі UV-Vis спектроскопії запропоновано й реалізовано оригінальний і простий метод моніторінгу кінетики утворення та виходу наночастинок металів у системах, де не проявляється смуга поверхневого плазмонного резонансу. З використанням цього підходу досліджено кінетику борогідридного відновлення солі Ni в чистій воді та в розчинах ПВС-*g*-ПАА залежно від концентрацій солі та кополімерних матриць. Встановлено ефекти підвищення початкової швидкості накопичення та виходу NiНЧ зі збільшенням концентрації солі Ni, а також зменшення обох параметрів у розчинах кополімеру порівняно з чистою водою. Водночас, швидкість акумуляції та вихід NiНЧ складним чином залежали від концентрації матриць, що визначалось співвідношенням таких факторів як зменшення швидкості дифузії молекул $NaBH_4$ в розчинах кополімеру та накопичення Ni^{2+}-іонів у частинках матриці завдяки комплексоутворенню з активними хімічними групами на першій стадії процесу відновлення. З використанням методу ТЕМ визначено морфологію та основні структурні елементи композиції NiНЧ/ПВС-*g*-ПАА. Показано, що *in situ* синтез NiНЧ у розчинах кополімеру супроводжується "від'єднанням" ПАА щеплень від основних ланцюгів ПВС і це призводить до появи нових структур, таких як "волохаті клубки" і "волохаті стержні", які містять малі сферичні NiНЧ (*d*~0,5–12,0 нм) в ізольованому та ланцюжковому стані відповідно. Виникнення останніх структур інтерпретовано з погляду утворення координаційних комплексів Ni^{2+}-іонів з активними групами обох ланцюгів ПВС і ПАА на першій стадії реакції відновлення.

Ключові слова: щеплений сополімер, наночастинки нікелю, процес відновлення, кінетика, морфологія.